# Near-field microwave microscopy on nanometer length scales

Atif Imtiaz,[a)] Marc Pollak, and Steven M. Anlage
*Center for Superconductivity Research, Department of Physics, University of Maryland, College Park, Maryland 20742-4111*

John D. Barry and John Melngailis
*Institute for Research in Electronics and Applied Physics, University of Maryland, College Park, Maryland 20742*

The Near-field scanning microwave microscope (NSMM) can be used to measure ohmic losses of metallic thin films. We report on the presence of an interesting length scale in the probe-to-sample interaction for the NSMM. We observe that this length scale plays an important role when the tip-to-sample separation is less than about 10 nm. Its origin can be modeled as a tiny protrusion at the end of the tip. The protrusion causes deviation from a logarithmic increase of capacitance versus a decrease in the height of the probe above the sample. We model this protrusion as a cone at the end of a sphere above an infinite plane. By fitting the frequency shift of the resonator versus height data (which is directly related to capacitance versus height) for our experimental setup, we find the protrusion size to be 3–5 nm. For one particular tip, the frequency shift of the NSMM relative to 2 μm away saturates at a value of about −1150 kHz at a height of 1 nm above the sample, where the nominal range of sheet resistance values of the sample is 15–150 Ω. Without the protrusion, the frequency shift would have followed the logarithmic dependence and reached a value of about −1500 kHz. © *2005 American Institute of Physics*. [DOI: 10.1063/1.1844614]

## INTRODUCTION

Near-field microwave and infrared techniques have proven useful for extracting material properties on the surfaces of many condensed matter systems for both fundamental and applied physics.[1,2] For example, on the fundamental physics side they have been used for quantitative imaging of dielectric permittivity, tunability, and ferroelectric polarization of thin dielectric films.[3] On the applications side they have been used to study electromagnetic fields in the vicinity of active microwave devices.[4] In near-field measurements, one often illuminates a probe with electromagnetic waves when the probe is held close to the surface of the sample. This probe-to-sample separation ($d$) is much less than the wavelength ($\lambda$) of the incident radiation. As a result, the electromagnetic fields are highly confined in space and are very sensitive to probe-sample separation. Due to this extreme sensitivity, sample topography and probe geometry often become convolved with the material properties of the sample. For most purposes, the information of interest is the material property. In order to deconvolve the required information, it is important that the probe geometry and topography effects are understood, so their effects can be eliminated.

The next important frontier of near-field measurements is to achieve a quantitative nanometer (nm) resolution imaging of material properties. One way of achieving high spatial resolution is to bring the probe to a height equal to the size of a few unit cells. This high spatial resolution is possible due to the extreme sensitivity of the electromagnetic fields on height. We have achieved near-field electromagnetic microscopy by integrating a scanning tunneling microscope (STM)

feedback circuit with a near-field scanning microwave microscope (NSMM), described in detail elsewhere.[5] This is similar to the other near-field microscopes utilizing STM to concentrate rf and microwave electric fields.[6–10] We have shown that our microscope is sensitive to the capacitance between the probe and sample as well as to the material properties of the sample.

The microwave microscope consists of a coaxial transmission line resonator coupled via a capacitor to the microwave source and feedback circuit.[5] The feedback circuit keeps track of the changes in resonant frequency of the resonator (producing a frequency shift signal, $\Delta f$) and the quality factor ($Q$) of the resonator. The probe end of the resonator has a sharp metal tip sticking out of it, and this same tip is used to do STM and microwave microscopy (see inset of Fig. 1). A simple lumped-element model for the probe-to-sample interaction is a capacitor $C_x$ (typical value ∼10 fF at a height of 1 nm) in series with a resistor $R_x$ in the case of conducting samples. The capacitance between the outer conductor and sample is so large that it presents a negligible impedance. The resistor contains the material information of interest in this case. One can employ a transmission line model for the microscope,[1] in which case the sample appears as a complex impedance given by $Z_x = R_x + 1/i\omega C_x$. In the limit $\omega C_x R_x \ll 1$, the resulting frequency shift ($\Delta f$) is independent of $R_x$ and is directly related to $C_x$ as $\Delta f/f_0 = -C_x/2C_0$, where $f_0$ is the resonant frequency of the unperturbed resonator and $C_0$ is the total capacitance of the microscope. In this case the microscope quality factor $Q$ contains the loss information of the sample. The validity of this
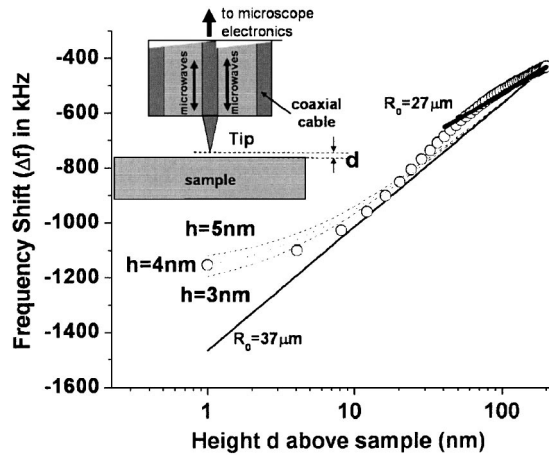
---

a)Electronic mail: aimtiaz@squid.umd.edu

FIG. 1. Frequency shift relative to 2-μm height of a coaxial microwave microscope vs tip-sample separation $d$. The sample is a boron-doped silicon substrate. The tip WRAP082 is used for measurements. The open circles show the frequency shift ($\Delta f$) data, solid lines are $\Delta f$ values calculated using capacitance values from the simple sphere above the plane model, dashed lines are $\Delta f$ values obtained from calculated capacitance values with a small cone added to a sphere of radius $R_0 = 37$ μm. Inset shows a schematic cross-section diagram of the very end of the microscope interacting with the sample (not to scale).



FIG. 2. Tunnel current [Ln ($I$) where $I$ is in nanoampere] vs $Z$ position for a STM tunnel junction between a Pt/Ir tip and Au/mica thin-film sample. The open squares are the data points and solid black line is the exponential fit with slope of $-0.41$ Å$^{-1}$. The bias on the film was 100 mV. The contact point is estimated using $I_{contact} = V_{bias}/R_{contact}$, where $R_{contact}$ is the expected point-contact resistance of 12.9 kΩ. This determines the distance of the tip to be 1 nm above the sample.

simple lumped-element treatment of the sample has been established for conducting films with low sheet resistance, i.e., in the limit $\omega C_x R_x \ll 1$.[11]

The probes we used are commercially available silver-coated tungsten tips. We find such tips to be good for both STM and NSMM. The measurement was performed on a variably boron-doped $n$-type silicon sample, doped with the focused ion beam (FIB) technique.[12] The energy of the boron beam was 30 keV, and it was used to dope a total area of $10 \times 10$ μm². At this beam energy the depth of boron implantation into silicon is approximately 100 nm.[13] After the ion-beam deposition the sample was rapid thermal annealed (RTA) to 900 °C in nitrogen for 20 s (5 s to ramp up the temperature, 10 s to anneal at 900 °C, and then 5 s to ramp down the temperature) to activate the carriers. This produced a roughly uniform dopant concentration over a thickness $t = 100$ nm. The area is doped in stripes with the same concentration along the 10-μm length and varying concentration in the perpendicular direction. The concentration varies from $10^{16} - 10^{21}$ ions/cm³ (resistivity $\rho = 10^{-2} - 10^{-6}$ Ω m) across this width, and there is a one to one relationship between concentration and resistivity for boron doping in silicon.[14] In this geometry, the resistivity can be converted to a sheet resistance given by $R_x = \rho / t$ (one can also write $R_x = 1/q\mu p$, where $q$ is the magnitude of the electron charge, $\mu$ is the mobility of holes, and $p$ is the dose of boron in ions/cm²) and the silicon substrate can be treated as a dielectric. This thin-film model works because the undoped silicon substrate has a resistivity of 0.61 Ω m, which is much larger than the doped film. The utility of this sample is that the surface is topography free and the only variations in the sample are due to the sheet resistance ($R_x$). This leaves our microwave signal mainly sensitive to material properties and probe geometry. The results reported in this paper satisfy the condition $\omega C_x R_x \ll 1$, since $R_x$ is in the range of 15–150 Ω, $\omega$ is
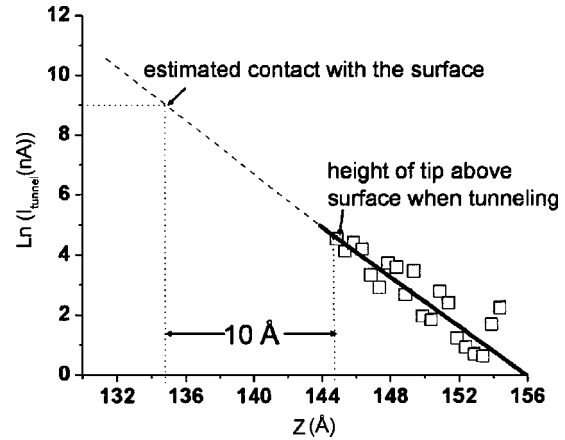
$2\pi 7.47 \times 10^9$ Hz, and $C_x$ is on the scale of $10^{-14}$ F. This gives the additional benefit that the microscope is sensitive mainly to the probe geometry, since $\Delta f$ is independent of $R_x$, as mentioned earlier.

As mentioned earlier, for nanometer spatial resolution, the height of the probe above the sample should be on the nanometer length scale as well. Here we estimate the probe-sample separation during constant tunnel current STM scanning. For a one-dimensional tunnel barrier between two metal electrodes, the tunneling current $I$ decays exponentially with the barrier width $a$, as $I \propto e^{-2\kappa a}$, where $\kappa = \sqrt{2m(V_B - E)/\hbar^2}$ and $E$ is the energy of the state and $V_B$ is the barrier potential. For vacuum tunneling, $V_B - E$ is just the work function of the metal.[15] For platinum (Pt) the work function is 5.65 eV, and $\kappa$ is on the order of $\sim 1$ Å$^{-1}$. We first demonstrate vacuum tunneling with data for a Pt/Ir tip over Au/mica sample, shown in Fig. 2. The tunnel current shows a clear exponential drop with probe-sample separation, having a slope of $-0.4$ Å$^{-1}$, on the order of that estimated for Pt. The $z$ position of the surface is estimated from the extrapolated point-contact current which is calculated through $I_{contact} = V_{bias}/R_{contact}$, where $V_{bias} = 100$ mV and $R_{contact}$ is taken to be 12.9 kΩ.[16] This estimate yields a nominal probe-sample separation of 1 nm during STM scanning.

Figure 1 shows representative data for the frequency shift versus height above a metallic sample between 1 nm and several hundreds of nanometers. We are able to study the detailed dependence of frequency shift versus height in the range below 100 nm. As shown by the data in Fig. 1, in this regime, we see a deviation from the expected logarithmic drop of the frequency shift versus height (which would appear as a straight line in Fig. 1). This deviation is quite generic and we have seen it over bulk metal, thin metal films, and semiconductors. In this paper, we attempt to understand the origin of this deviation.

To perform the STM on doped silicon, the bias on the sample was +1 V and the tunnel current set point for STM feedback was 0.5 nA. Such high bias is needed in order to

overcome the ~0.7 V of voltage drop across the buried *p-n* junction of the boron-doped silicon. The microwave source frequency was 7.472 GHZ and the power level was +3 dBm. This power level was chosen to avoid rectification of the microwave signal in the STM tunnel junction, which is seen for powers above +5 dBm.

## MODEL

As mentioned earlier, experimentally, the very end of the microwave probe is coaxial with the inner conductor protruding beyond the end of the coaxial cable (inset of Fig. 1). The protruding section of the inner conductor has a roughly conical geometry. The same tip is used for STM and electromagnetic wave illumination and concentration. To determine the capacitance between the probe and sample, one can model a conical tip sticking out of the inner conductor of the coax and calculate its capacitance with respect to a conducting plane. On millimeter and micron length scales, the outer conductor of the coax has to be taken into account in order to correctly calculate the probe-sample capacitance. However, our interests are for measurements in the submicron height regime, where the outer conductor capacitance does not change significantly. One option is to model the tip as an infinite cone. However, an infinite cone above a sample is a scale invariant problem, as it puts no length scale for the probe itself. We will model the probe as a sphere above a sample, where the sample is an infinite plane.[17] Such a model gives another length scale, which is the sphere radius $R_0$, in addition to the height ($d$) of the probe (measured from the bottom of the sphere to the flat sample) above the infinite plane.

This model has been applied earlier to study the behavior of microwave microscopes on submicron length scales, however, far away from the atomic length. The strength of this model lies in its analytic expressions for capacitance and static electric field, obtained through an image charge method. This model has also been successfully extended to understand the dynamics of electromagnetic interactions between probe and sample.[17] However, in this paper we limit ourselves to the static aspects.

Electromagnetically speaking, the tip-to-sample interaction in our microwave microscope is very complex, and modeling it analytically alone is a very challenging task. We resort to numerical techniques when analytic models become difficult. For example, the addition of even a small object at the end of the probe makes the analytic problem very complex to solve. The numerical modeling was performed with a commercially available ANSOFT MAXWELL 2D (M2D) software, which solves a variety of static electric and magnetic problems. We model the measured nanometer scale deviations by adding a small geometrical object (a tiny cone) at the end of the sphere. The height of the cone is "$h$" and the cone and sphere together act as a probe above the sample.

## RESULTS

Our goal is to understand the $\Delta f$ versus height above the sample data for heights below 10 nm, as shown for a representative case in Fig. 1. For heights above 10 nm, the inter-
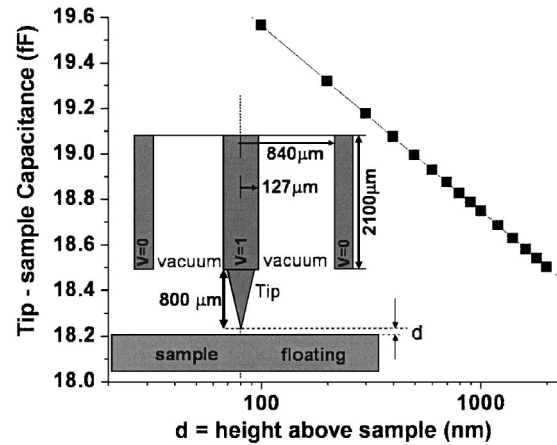


FIG. 3. Tip-to-sample capacitance from MAXWELL 2D (M2D) for the coaxial probe geometry shown in cross section in the inset. The outer conductor is included in the model and the different voltages (V in volts) and lengths are shown on the drawing in the inset (not to scale). The plot shows the logarithmic drop of capacitance with increasing $d$ calculated from this model. The tip is conical except for last 14.2 μm which is an ellipsoid with a flat bottom facing the sample. The box size for the problem was $2500 \times 2100$ μm$^2$.

pretation is simple as one gets close to the sample. The effective area of the parallel-plate capacitor is changing at the same time as the distance $d$ is changing. In Fig. 1, we show this by two solid lines for the analytic sphere above the plane model. A sphere of $R_0 = 27$ μm describes the data at large heights ($d > 50$ nm), and a sphere of radius $R_0 = 37$ μm works well as one gets closer to the sample. However, this trend changes below 10 nm where we see saturation in the $\Delta f$ signal, and this saturation is seen above all samples measured so far. What follows here is a systematic discussion to understand this saturation.

First we start with a model which is closest to the experiment. Figure 3 is a plot of capacitance versus height for a coaxial probe with conical tip above a conducting sample, determined numerically using MAXWELL 2D (M2D). The geometrical model is shown in cross section in the inset of Fig. 3. The center conductor was set at a potential of 1 V, the outer conductor was set to 0 V, and the sample was left to float. Here we use the approximation that the near-field structure will be dictated by the static electric-field structure. This approximation is valid, since in our case the source (probe tip) and sample separation satisfy the condition $d \ll \lambda$; where we assume that electromagnetic sources and fields have harmonic ($e^{-i\omega t}$) dependence. With this assumption one can write down the equations for the potentials and the fields as a function of position and time. After integration over time, the final solution for fields in the "near zone" ($d \ll \lambda$) shows the quasistatic nature of the fields.[18]

The key point to note in Fig. 3 is that the probe-to-sample capacitance for a conical tip has a logarithmic increase as a function of decreasing height, even in the submicron regime. Any model that we use should maintain this qualitative behavior. Due to aspect ratio limitations of the M2D software (ratio of largest length scale to smallest must be less than ~$10^3$), we were not able to push this study to much smaller separation, $d$. However, the sphere above an infinite plane model can be taken to these small length scale
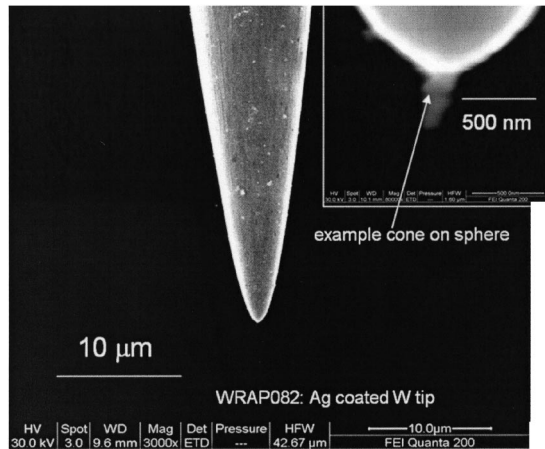
FIG. 4. Scanning electron microscope micrograph for one of the STM probe tips, WRAP082. Inset shows the magnification of the apex of the tip, which illustrates the cone-shaped particle sticking to the probe. This tip was imaged before use in the NSMM.

values in M2D, since $R_0$ is much smaller than the dimensions of the full coaxial probe and we have more room to work around aspect ratio problems. However, before we discuss that, it is better to examine the geometry of the tips used.

### Geometry of the probes

The metal tips in our experiment are first imaged by a scanning electron microscope (SEM), where they reveal a rounded conical nature (Fig 4). On the millimeter and micrometer length scale, the probe can be well approximated as a cone. Near the tip, the cone is rounded and includes a sphere of radius $r$. Note the protrusion sticking out of the tip, shown in the inset of Fig. 4. This small protrusion is probably left from the tip preparation procedure. The size of protrusion at the apex of the tip is few hundred nanometers (see the inset of Fig. 4) in this case. In general, the tip can pickup material from the sample, and there can be other sources of damage. Protrusions like this can have a significant effect on the measurement.

A second observation is that the tip-sample capacitance (as measured through $\Delta f$) is proportional to the included sphere radius $r$. On the submicron scale one can easily see an effective sphere with radius "$r$" (this $r$ is distinct from $R_0$) embedded at the end of the probe, as illustrated in Fig. 5(b). For the probes shown in the figure the approximate $r$ value is 6 $\mu$m (commercial name WRAP30D) and 8 $\mu$m (commercial name WRAP30R). Figure 5(a) shows that as $r$ gets larger, the magnitude of the frequency shift signal between tunneling height and 2 $\mu$m (defined as $\overline{\Delta f}$) gets larger. Here the sample is a gold thin film on mica satisfying $\omega C_x R_x \ll 1$, so in this case the total frequency shift $\overline{\Delta f}$ is directly proportional to capacitance change. We arbitrarily define the zero of $\overline{\Delta f}$ to be the height of 2 $\mu$m. These data illustrate the dramatic dependence of the frequency shift (and capacitance change) on probe dimension, and help justify modeling of the probe as a sphere, at least on submicron length scales. However, the tips of large $r$, which show a dramatic change of frequency shift signal, are generally very poor for STM.
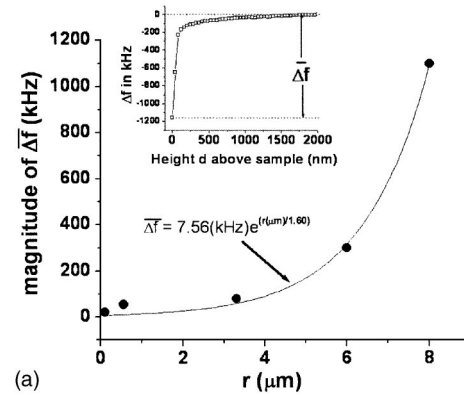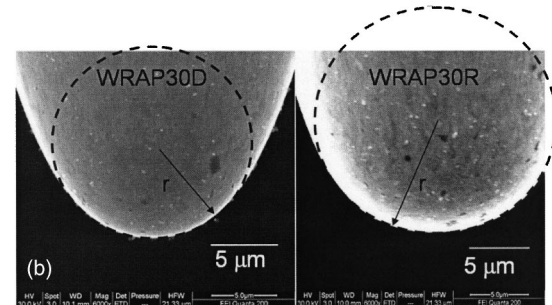




FIG. 5. (a) Magnitude of the frequency shift of the NSMM between tunneling height and 2 $\mu$m (defined as $\overline{\Delta f}$) on a gold/mica thin-film sample vs inscribed sphere radius $r$ on the tip. Note that $\overline{\Delta f}$ increases roughly exponentially (solid line) with increasing $r$ for different probes (inset shows the definition of magnitude of $\overline{\Delta f}$) and (b) SEM micrograph showing inscribed sphere radius $r$ for two different probes WRAP30D ($r \approx 6$ $\mu$m) and WRAP30R ($r \approx 8$ $\mu$m).

These tips enlarge the topographic features laterally (which can happen if the tip has multiple tunneling sites) and give incorrect heights of known features as well.

### Discussion of results for sphere above plane

Figure 6 is a plot of the capacitance of a sphere above an infinite plane calculated two different ways (analytic and numerical), as the height is varied. It also clearly shows the logarithmic increase of capacitance versus decreasing height, for both the analytical model (solid line) and numerical model (points). This simple model thus preserves the logarithmic dependence observed in Fig. 3. The slopes are very close to each other (differing by only 1.3%). The offset of the numerical curve is due to the limited size of the numerical simulation. Figure 7 shows the numerically determined capacitance versus the inverse of the numerical problem size (area of drawing in M2D, called the box size) for different fixed heights above a conducting sample. It shows that in the limit of infinite box size, the extrapolated numerical result agrees with the analytic result to within 1.4%. For example, for the height of 1 nm, the analytic value of capacitance is 25.23 fF. In the limit of infinite box size, M2D yields a value of 25.58 fF (the graph also shows a comparison for two other heights).

We note that the sphere radius $R_0$ required to fit the $\Delta f(d)$ data (like that in Fig. 1) is much larger than the embedded sphere radius $r$. This is because the embedded sphere intercepts only a fraction of the electric-field lines between
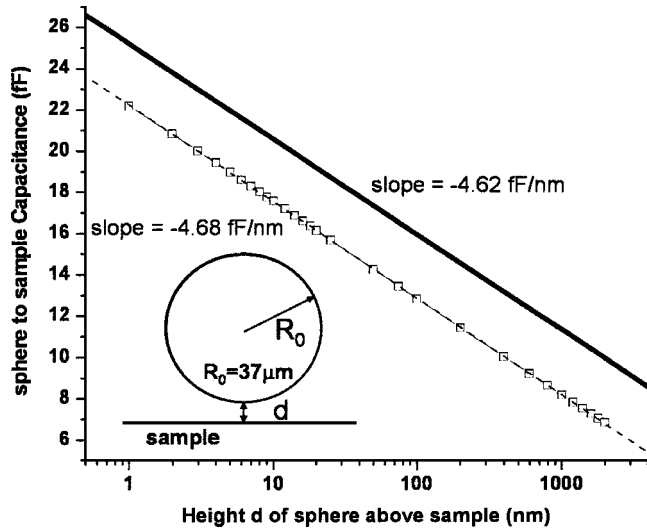
FIG. 6. Comparison of sphere to sample capacitance (inset shows the geometry) calculated from the analytic model (solid line) and M2D (data points). The sample is infinite in the analytic case. The sphere radius $R_0$ =37 $\mu$m. The box size for M2D is $90 \times 91$ $\mu$m$^2$. The boundary condition on the box was Neumann (electric field tangent to the boundary of the box). The slopes agree to within 1.3%.

the tip and the sample, thus missing the field lines between the rest of the nonspherical probe and sample. The net effect of all these field lines is incorporated in an artificially enhanced $R_0$ for the model sphere. We find that the value of $R_0$=37 $\mu$m fits our data best for heights down to 10 nm, for the tip shown in Fig. 1.

## Discussion of results with small cone added to sphere above the plane

In order to study the deviation of our tips from spherical shape, we added a small cone at the end of the sphere (inset of Fig. 8). This is motivated partly by the cone-shaped "particle" seen in the SEM micrograph (shown in the inset of Fig. 4). We find (numerically) that other shapes produce
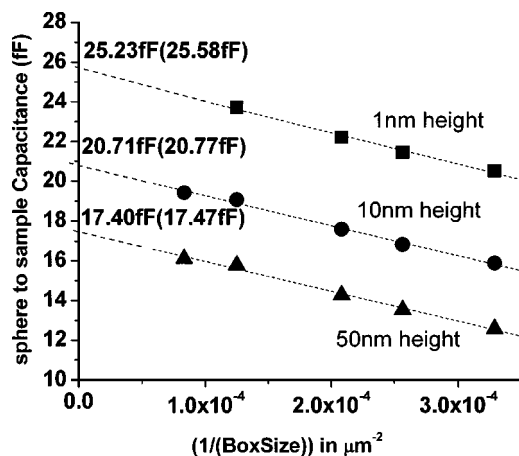


FIG. 7. Comparison of sphere to sample capacitance as a function of inverse box size of the M2D calculation. The numbers in parentheses show the projected value of capacitance that M2D would yield in the limit of infinite box size (i.e., the *y* intercept of the straight line fits). The extrapolated values are within 1.4% of the analytic values (shown outside of parentheses) at the same height.
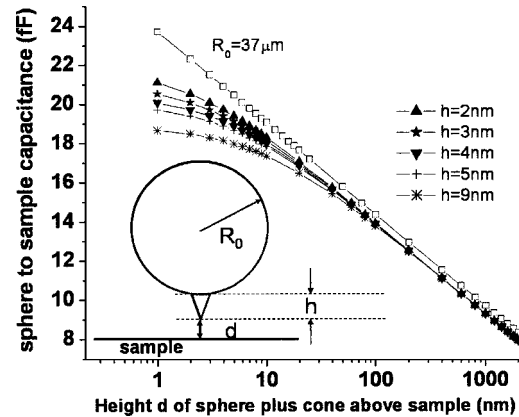


FIG. 8. Sphere (with radius of $R_0$=37 $\mu$m) to sample capacitance with a small cone of height *h* and base 2 nm added at the end of the sphere using M2D (inset shows the geometry, which is not to scale). The capacitance saturates at heights *d* on the same scale as *h*. Plot shows results for several different values of the cone size *h*. The box size is $80 \times 81$ $\mu$m$^2$. The boundary condition on the box was Neumann (electric field tangent to the boundary of the box).

similar results. This cone has two lengths associated with it, namely, the base and height of the cone. We found that the height of this cone is the only key parameter affecting the overall capacitance, so we took the base to be fixed (2 nm) for all the heights. This model was studied numerically, since the analytic problem with this perturbation (cone) is difficult to solve. As shown in Fig. 8, adding this perturbation produces a deviation from the logarithmic increase of capacitance with decreasing height. The effect on the capacitance sets in at heights on the same length scale as the size of the cone, and it tends to saturate the capacitance. The larger the value of *h*, the more prominent is the saturation effect.

In Fig. 1, the dotted curves show these capacitance values converted into frequency shift using a transmission line model of the microscope.[1,11] The frequency shift data are plotted as open dots for comparison. We find that a sphere of radius $R_0$=37 $\mu$m with a perturbation cone height of 3–5 nm fits the data well. This shows that a real tip can be modeled fairly well by a conducting sphere, and even the deviations from the sphere above the plane model can also be understood by adding small perturbations to the sphere.

## CONCLUSION

We report an interesting length scale in tip-to-sample interaction for near-field microwave measurements. The origin of this length scale is a deviation of the probe geometry from an ideal (spherical or conical) geometry. This length scale is typically on the order of 3–5 nm and will effect measurements on these length scales. Such results are important to design an optimum probe for the future development of near-field microwave microscopes.

## ACKNOWLEDGMENTS

[1] S. M. Anlage, D. E. Steinhauer, B. J. Feenstra, C. P. Vlahacos, and F. C. Wellstood, in *Microwave Superconductivity*, edited by H. Weinstock and M. Nisenoff (Kluwer, Dordrecht, 2001), Chap. 10, p. 239.

[2] B. T. Rosner and D. W. van der Weide, Rev. Sci. Instrum. **73**, 2505 (2002).

[3] D. E. Steinhauer, C. P. Vlahacos, F. C. Wellstood, S. M. Anlage, C. Canedy, R. Ramesh, A. Stanishevsky, and J. Melngailis, Rev. Sci. Instrum. **71**, 2751 (2000).

[4] S. M. Anlage, C. P. Vlahacos, S. Dutta, and F. C. Wellstood, IEEE Trans. Appl. Supercond. **7**, 3686 (1997).

[5] A. Imtiaz and S. M. Anlage, Ultramicroscopy **94**, 209 (2003).

[6] G. P. Kochanski, Phys. Rev. Lett. **62**, 2285 (1989).

[7] W. Seifert, W. Gerner, M. Stachel, and K. Dransfeld, Ultramicroscopy **42–44**, 379 (1991).

[8] B. Michel, W. Mizutani, R. Schierle, A. Jarosch, W. Knop, H. Benedickter, W. Bachtold, and H. Rohrer, Rev. Sci. Instrum. **63**, 4080 (1992).

[9] S. J. Stranick and P. S. Weiss, Rev. Sci. Instrum. **65**, 918 (1994).

[10] B. Knoll, F. Keilmann, A. Kramer, and R. Guckenberger, Appl. Phys. Lett. **70**, 2667 (1997).

[11] D. E. Steinhauer, C. P. Vlahacos, S. K. Dutta, B. J. Feenstra, F. C. Wellstood, and S. M. Anlage, Appl. Phys. Lett. **72**, 861 (1998).

[12] J. Melngailis, J. Vac. Sci. Technol. B **5**, 469 (1987).

[13] R. G. Wilson and G. R. Brewer, *Ion Beams with Applications to Ion Implantation*, 1st ed. (Wiley, New York, 1973), Chap. 4, p. 272.

[14] S. M. Sze, *Physics of Semiconductor Devices*, 1st ed. (Wiley, New York, 1969), Chap. 2, p. 43.

[15] J. Tersoff and N. D. Lang, in *Scanning Tunneling Microscopy*, 1st ed., edited by J. A. Stroscio and W. J. Kaiser (Academic, San Diego, 1993), Vol. 1, Chap. 1, p. 1.

[16] N. D. Lang, Phys. Rev. B **36**, 8173 (1987).

[17] C. Gao, F. Duewer, and X. D. Xiang, Appl. Phys. Lett. **75**, 3005 (1999); U.S. Patent No. 6,532,806 (18 March 2003).

[18] J. D. Jackson, *Classical Electrodynamics*, 3rd ed. (Wiley, New York, 1999), Chap. 9, p. 408.